8-2012

Convolution Backprojection for SAR Image Formation

Timothy P. Ray
University of Texas-Pan American

CONVOLUTION BACKPROJECTION FOR SAR IMAGE FORMATION

A Thesis

by

TIMOTHY P. RAY

Submitted to the Graduate School of the
University of Texas-Pan American
In partial fulfillment of the requirements for the
degree of

MASTER OF SCIENCE

August 2012

Major Subject: Mathematical Sciences

CONVOLUTION BACKPROJECTION FOR SAR IMAGE FORMATION

A Thesis
by
TIMOTHY P. RAY

COMMITTEE MEMBERS

Dr. Zhijun Qiao
Chair of Committee

Dr. Andras Balogh
Committee Member

Dr. Zhaosheng Feng
Committee Member

Dr. Eleftherios Gkioulekas
Committee Member

August 2012

ABSTRACT

Ray, Timothy P., Convolution Backprojection for SAR Image Formation. Master of Science (MS), August, 2012, 48 pp., 14 figures, references, 39 titles.

Convolution Back Projection (CBP) is an imaging algorithm, which can be applied to data gathered by a Synthetic Aperture Radar (SAR) system to produce high resolution images. The Mathematics of CBP was first studied in the context of tomographic image reconstruction for medical applications. CBP image processing has also been applied to a variety of other fields, such as seismic imaging, sonar, and radio astronomy. In terms of SAR image processing algorithms, CBP is far less efficient than direct Fourier Inversion Algorithms. The purpose of this thesis is to study the CBP algorithm as it is applied to SAR image formation. Specifically, thesis will provide the formulation of the CBP algorithm for a circular SAR geometry. The starting point for the development of this algorithm is a common radar wave model, which can be derived from Maxwells Equation's.

DEDICATION

This thesis is dedicated to my parents David and Katherine, and to my brother and sisters. Thank you for all your love and support. Most importantly, I give all the glory to my Lord and Savior Jesus Christ, at whose feet I lay all of my accomplishments.

ACKNOWLEDGMENTS

I am grateful to my advisor Dr. Zhijun Qiao for all of his help over the past two years. This work was partially supported by the US Department of Defense Army Research Office under grant number W911NF-08-1-0511, and by the Norman Hackerman Advanced Research Program under grant number 003599- 0001-2009.

TABLE OF CONTENTS

LIST OF FIGURES

CHAPTER I

INTRODUCTION

Radar is an acronym that stands for Radio Detection and Ranging. It is a remote sensing technology that uses electromagnetic radiation in the radio or microwave spectrum to detect objects over large distances. From its name, it should be clear that a true radar system must be able to both detect a target and determine its distance from the radar antenna. However, modern systems have a number of other added capabilities. For example, some radar systems are able to measure the velocity of a target in terms of the doppler-shift induced by the motion of the target, which may be either linear or rotational. Another very important application of radar is the production of high resolution images.

It is the application of radar technology to the image formation problem that will be the subject of this this thesis. Specifically the application of convolution backprojection (CBP) to the problem of radar imaging will be considered. The most common radar imaging technology that is currently in use is synthetic aperture radar (SAR), which uses the motion of the radar antenna with respect to a stationary target to improve image resolution when compared to a stationary antenna. These techniques discussed in this thesis can also easily be applied to a similar imaging problem where the target is moving and the antenna is stationary. This method is referred to as inverse synthetic aperture radar (ISAR).

The CBP is algorithm is a computerized tomographic imaging technique that was originally developed for medical imaging applications. This imaging method has since been expanded to a variety of different fields. These include radio astronomy, geophysics, and sonar. The application of the CBP to radar is a relatively new development, dating to the middle of the1980s. Prior to the introduction of backprojection algorithms, the primary method used in radar image reconstruction were direct Fourier techniques such as the polar format algorithm.

The purpose of this thesis is to study the CBP algorithm as it is applied to SAR image formation. This algorithm will be formulated based on a common radar wave model, which can be derived from Maxwells Equations. In specific, a formulation of the CBP algorithm for the case of a circular SAR system will be presented. The key to development that will be used to formulate the CBP algorithm is the projection-slice theorem.

I.1 Thesis Chapter Outline

Here a basic outline of the thesis chapters is presented.

Chapter 2:

An introduction to SAR and the two of most important imaging modes will be discussed. Next, a discussion of signal processing will be presented. Finally, the linear chirp signal will be introduced.

Chapter 3:

A Mathematical Model for the signal received by a monostatic radar antenna will be developed. The development of this model will begin with Maxwell's equations. From these the scalar wave equation will be derived. A model for radar wave propagation will then be determined based on the solution to the scalar wave equation.

Chapter 4:

First, the radar path geometry for a Circular-SAR system will be defined. Next, the model for the received signal will be refined in terms of the assumption that the distance from the antenna to the target center is large in comparison to the target scene size. Finally, it will be shown that the received radar can be considered to be a two dimensional Fourier transform, and the data collection in the wave number domain will be considered.

Chapter 5:

An inversion method for the collected SAR data will developed based on the projection-slice theorem. A brief discussion of the Radon and x-ray transforms will first be presented, followed by a presentation of the projection-slice theorem.

Chapter 6:

The Inversion method in chapter 5 will be used to develop a CBP algorithm. A set of Matlab simulations for this algorithm will then be shown.

CHAPTER II

SAR PRELIMINARIES / SIGNAL PROCESSING

II.1 Sythetic Aperture Radar (SAR)

Synthetic aperture radar (SAR) is a remote sensing technique that uses an antenna, which is mounted on a moving platform, to image a stationary target scene. In most cases, SAR antennas are either mounted on airborne or spaceborne platforms, such as airplanes or satellites. These antennas use highly directed microwave radiation to produce images of specific patch of the Earth's surface. Unlike most remote imaging systems such as visible and infrared systems, SAR uses active imaging [10, 18]. This means that the portion of the ground that is to be imaged must first be illuminated by a beam of microwave energy emitted by a transmitting antenna, rather than relying on passive sources of illumination such as solar radiation. SAR systems are also preferred over other types due to their ability to produce high quality images through cloud cover and at night [9].

In the early 1950's, Carl Wiley discovered a novel method to increase the cross-range resolution of radar imaging systems, which he referred to a doppler beam sharpening [39]. What he discovered was that a comparison of the returns from a series of radar pulses from an antenna mounted on a platform moving along a given flight path parallel to the ground could be used to produce a higher resolution image [5]. In this way, a synthetic aperture with length equal to that of the platform flight path is created. The method that he discovered was essentially the same as what is now called stripmap-mode SAR.

The purpose of this thesis is to study the CBP algorithm as it is applied to SAR image formation. This algorithm will be formulated based on a common radar wave model, which can be derived from Maxwells Equations. In specific, a formulation of the CBP algorithm for the case of a circular SAR system will be presented. The key to development, which will be used to formulate the CBP algorithm, is the projection-slice theorem.

Figure II.1: SAR Image of the Washington DC area

II.2 SAR Imaging Modes

There are a number of different types of SAR imaging systems that are currently in use. Two of the most common SAR modes, which are used by modern systems, are stripmap-mode and spotlight-mode. However, it should be noted that these modes are not exclusive. That is, there are some SAR systems that can switch between imaging modes [9].

As was previously mentioned, the original SAR mode that was invented by Wiley was stripmap-mode SAR. In the case of this SAR mode, the radar antenna is mounted at a fixed angle on a moving platform. stripmap-mode SAR systems are capable of producing high resolution images over a large region of the ground. This makes it useful for terrain mapping.

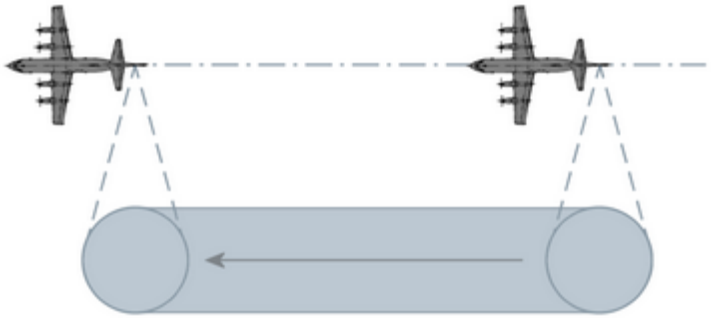

Figure II.2: Illustration of stripmap-mode SAR

In the case of Spotlight-mode SAR, the radar beam is steered so that it remains focused on a single area of the target space. Spotlight-mode SAR systems can use either electronic or mechanical beam steering [36]. The main advantage of this mode is that it has increased image resolution when compared to stripmap-mode SAR. However, this increase in resolution comes at the cost of decreased area coverage. It is spotlight-mode SAR that is most commonly associated with the CBP imaging algorithm.

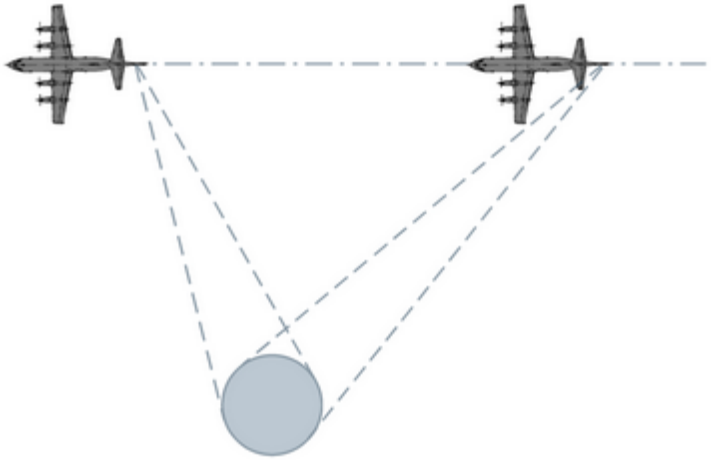

Figure II.3: Illustration of spotlight-mode SAR

II.3 Sampling Considerations

Modern radar data processing is performed by computers. For this reason, it is necessary to employ various sampling methods to produce discrete data sets from continuous signals. In order for any

sampling method to be useful, the original signal should be able to be recovered from the sampled data set through interpolation. The ability of a particular sampling method to accurately recreate a given signal depends on length of the sampling interval T_s. The sampling interval must be sufficiently small in order for the signal to be recoverable.

For a band- limited signal, sampling corresponds to the repetition of the signals spectrum at intervals of $f_s = 1/T_s$. The sampling rate must be chosen such that there is no overlap in the repeated spectrum of the sampled signal. For real valued band-limited signals, the sampling rate must be chose such that the sampling frequency is greater than twice the bandwidth of the signal. This requirement is referred to as the Nyquist sampling rate[32].

How the bandwidth of a signal is determined depends on whether that signal is real or complex valued. The Fourier Transform of a real valued signal is always an even function. For this reason, the portions of the signal determined by the positive and negative frequencies will be mirror images of one another. Thus, the bandwidth is given by $f_{\text{max}} - f_{\text{min}}$, where f_{max} and f_{min} are the largest and smallest positive frequency component of a given signal [9]. On the other hand the bandwidth of complex signals is determined by both the negative and positive frequency components.

All radar signals are real valued; however, there are a number of sampling methods that treat a real valued signal as the real part of a complex signal. The key advantage of such complex sampling methods is that the Nyquist rate is relaxed so that the minimum sampling rate required to recover the original signal is equal to the bandwidth. In this case, each sample contains twice the amount of information when compared to a real valued sample.

There are a number of different ways in which a real valued time varying signal $s(t)$ can be transformed into a complex signal for sampling purposes. One such method involves the Hilbert transform, which is defined as follows

$$\mathcal{H}\{s\} = \frac{1}{\pi} \int_{\mathbb{R}} \frac{s(\tau)}{t-\tau} d\tau. \tag{II.1}$$

A complex signal $\widetilde{s}$ can then be defined such that

$$\widetilde{s}(t) = s(t) + i\mathcal{H}\left\{s\right\}(t). \tag{II.2}$$

The spectrum of the Hilbert pair of $s(t)$ is given by $\mathscr{F}\left\{\mathcal{H}\left\{s\right\}\right\} = -i\text{sgn}(f)S(f)$. Thus, the spectrum of $\widetilde{s}$ is given by

$$\mathscr{F}\left\{\widetilde{s}\right\} = \begin{cases} 2S(f) & f \geq 0, \\ 0 & f < 0. \end{cases} \tag{II.3}$$

This shows that combining the original signal with its Hilbert pair, as illustrated by (II.2), generates a new signal that is only nonzero on the positive portion of the spectrum. This new signal can then be sampled at a greater rate than the reduced Nyquist rate for complex signals.

The Hilbert transform method is not generally used in actual radar imaging applications, since for many types of signals there is no practical method of implementing the Hilbert transform [2]. However, a good approximation can be found for an FM signals of the form $p(t) = a(t)\cos(2\pi f_c t)$, where f_c is again the carrier frequency. This can be accomplished by noting that $\cos(2\pi f_c t)$ and $\sin(2\pi f_c t)$ are Hilbert pairs. The imaginary part of the new signal is referred to as the quadrature component, which is given by $q(t) = a(t)\sin(2\pi f_c t)$. Then, the real valued signal $p(t)$ can be sampled in terms of the following complex signal.

$$s(t) = p(t) + iq(t) = a(t)e^{i2\pi f_c t}. \tag{II.4}$$

Unlike the Hilbert sampling case, signals which are in the quadrature form given in (II.4) may have negative frequencies. However, in cases where the carrier frequency is chosen to be larger than the bandwidth, only positive frequencies will be considered.

II.4 Chirp Signal

On type of signal that is commonly used in radar imaging application is a linear chirp signal, with limited time duration T, which is given by the following form:

$$\begin{aligned} p(t) &= \text{rect}\left(\frac{t}{T}\right) e^{i\pi K t^2} e^{i2\pi f_c t} \\ &= \text{rect}\left(\frac{t}{T}\right) e^{i\Phi(t)}, \end{aligned} \tag{II.5}$$

where

$$\text{rect}(t) = \begin{cases} 1 & -\frac{1}{2} \leq t \leq \frac{1}{2} \\ 0 & \text{otherwise} \end{cases}.$$

Here $p(t)$ is assumed to be a frequency modulated signal with a carrier frequency f_c and K denotes the chirp rate. Also, let $\Phi(t) = \pi K t^2 + 2\pi f_c t$ denote the phase function.

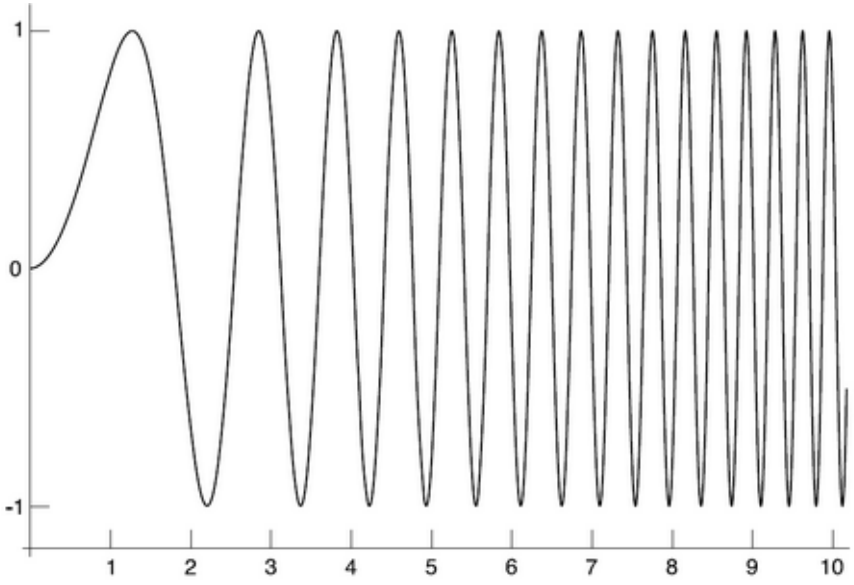

Figure II.4: Chirp Signal

The chirp signal p given in (II.5) has an instantaneous frequency component that varies linearly with time, as is shown below

$$f_{in} = \frac{1}{2\pi}\frac{d}{dt}\Phi(t) = Kt - \tilde{f}. \tag{II.6}$$

This is the reason that $p(t)$ is referred to as a linear chirp signal. The primary advantage of this type of signal, when compared to a pulse with constant frequency, is that they are able to produce high range resolution images with longer pulse duration [21]. It should be noted, that the longer duration pulses are useful because their peak power is higher. This extends the range of such a pulse. Generally, a signal processing method known as pulse compression will be used to further improve range resolution by artificially shortening the pulse duration. This method will be discussed further in chapter IV.

Thus, in order to ensure that such a signal has a finite bandwidth, it is necessary to restrict the signal to a finite time interval. It is reasonable to assume that the bandwidth of p will primarily depend on the chirp rate K and the duration of the pulse given by T. In order to show that this is true in a rigorous manner, the spectrum of p needs to be found. To this end, consider that the Fourier transform of p is given by

$$\begin{aligned} P(f) = \mathcal{F}\{p\} &= \int_{-\infty}^{\infty} \text{rect}\left(\frac{t}{T}\right) e^{i\pi K t^2} e^{-i2\pi(f-f_c)t} dt \\ &= \int_{-\infty}^{\infty} \text{rect}\left(\frac{t}{T}\right) e^{i\Psi(t)} dt. \end{aligned} \tag{II.7}$$

where Ψ is the phase function given by$\Psi(t) = \pi K t^2 - 2\pi \tilde{f} t$, and $\tilde{f} = f - f_c$.

This integral can be evaluated using the method of stationary phase, as is done in [18]. Using this method, the spectrum of $p(t)$ is shown to be

$$P(f) \approx \frac{1}{\sqrt{K}} \text{rect}\left(\frac{f-f_c}{K \cdot T}\right) e^{-i\frac{\pi(f-f_c)^2}{K}} e^{i\frac{\pi}{4}}. \tag{II.8}$$

The power spectrum of the chirp signal can now be approximated by

$$|P(f)|^2 \approx \frac{1}{K} \text{rect}\left(\frac{f-f_c}{K \cdot T}\right).$$

This shows that the power of a chirp signal of the form given in (II.5) has a neglagible power

outside of the support interval $\left[f_c - \frac{f_B}{2}, f + \frac{f_B}{2}\right]$. Hence, $f_B = K \cdot T$ is the finite bandwidht of the signal.

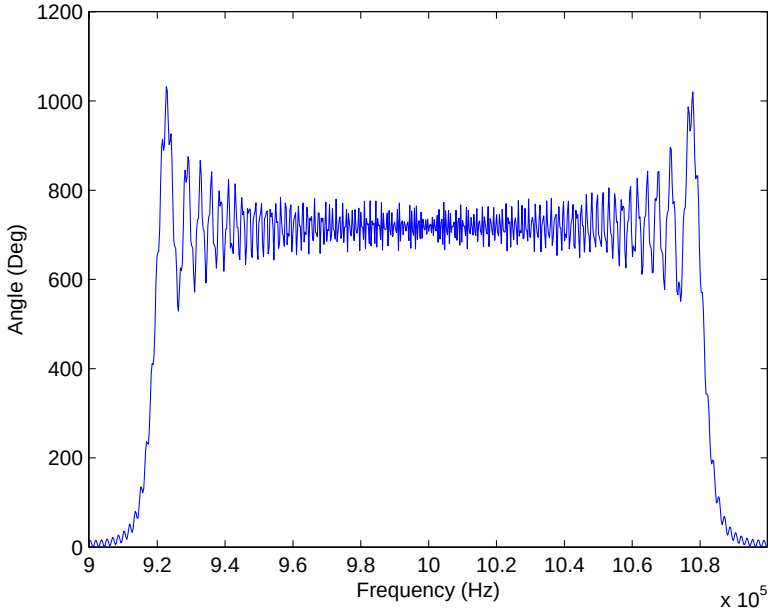

Figure II.5: Power Spectrum of a Chirp Pulse with a bandwidth of 2×10^5 Hz

CHAPTER III

RADAR WAVE PROPAGATION MODEL

III.1 Maxwell's Equations

In this section, a model for the propagation of radar signals in free space is derived. As was mentioned in previous sections, radar signals are a form of electromagnetic radiation. These signals are produced by a current on a single isotropic antenna located at $\mathbf{x}_0 \in \mathbb{R}^3$. This antenna will serve both as the transmitting and as the receiving antenna. When these waves come into contact with a target, a current is induced, which causes a weaker scattered form of the signal to be retransmitted.

The proper model for electromagnetic waves propagation is based on Maxwell's equations, which are listed below.

$$\boldsymbol{\nabla} \times \mathbf{E} = -\partial_t \mathbf{B}, \tag{III.1a}$$

$$\boldsymbol{\nabla} \times \mathbf{H} = \mathbf{J} + \partial_t \mathbf{D}, \tag{III.1b}$$

$$\boldsymbol{\nabla} \cdot \mathbf{E} = \rho, \tag{III.1c}$$

$$\boldsymbol{\nabla} \cdot \mathbf{B} = 0. \tag{III.1d}$$

The quantities given in the above equations are:

- $\mathbf{D}(t, \mathbf{x})$ - electric displacement field
- $\mathbf{E}(t, \mathbf{x})$ - electric field
- $\mathbf{B}(t, \mathbf{x})$ - magnetic induction field
- $\mathbf{H}(t, \mathbf{x})$ - magnetic field
- $\mathbf{J}(t, \mathbf{x})$ - current density

- $\rho(t, \mathbf{x})$ - charge density

The electric displacement field and the electric field, and the magnetic induction field and the magnetic field are related by

$$\mathbf{B} = \mu\mathbf{H} \qquad \text{and} \qquad \mathbf{D} = \epsilon\mathbf{E}.$$

Here, the coefficients in the above equations are defined by

- $\mu(\mathbf{x}, t)$ - the permeability of the medium of propagation
- $\epsilon(\mathbf{x}, t)$ - permittivity of the medium propagation

In many cases, the following set of non-homogeneous scalar wave equations can be used to model radar waves in place of Maxwells equations

$$\left(\boldsymbol{\nabla}^2 - \frac{1}{c_0^2}\partial_t^2\right)\mathbf{E}(t, \mathbf{x}) + \mu_0\partial_t\mathbf{J}(t, \mathbf{x}), = 0 \tag{III.2a}$$

$$\left(\boldsymbol{\nabla}^2 - \frac{1}{c_0^2}\partial_t^2\right)\mathbf{H}(t, \mathbf{x}) + \nabla \times \mathbf{J}(t, \mathbf{x}) = 0. \tag{III.2b}$$

It is possible to model radar waves in terms of either equation, but it is customary to use the electric field, as in III.2a.

In order to derive the above equations, it must be assumed that radar wave propagation mostly occurs in free space. This will serve as a good approximation of radar waves as they travel through the air. The only exception will be that for $\mathbf{x} = \mathbf{x}_0$, the current density $\mathbf{J}(t, \mathbf{x}) \neq \mathbf{0}$. Otherwise, $\mathbf{J}(t, \mathbf{x}) = \mathbf{0}$. In addition, $\rho(t, \mathbf{x}) = 0$ for all $\mathbf{x} \in \mathbb{R}^3$. Based on these assumptions, the following

variants of (III.1a), (III.1b), and (III.1c), which will be used to derive the (III.2a), can be found

$$\boldsymbol{\nabla} \times \mathbf{E} = -\partial_t \mathbf{B}, \tag{III.3a}$$

$$\boldsymbol{\nabla} \times \mathbf{B} = \mu_0 \mathbf{J} + \mu_0 \epsilon_0 \partial_t \mathbf{E}, \tag{III.3b}$$

$$\boldsymbol{\nabla} \cdot \mathbf{E} = 0. \tag{III.3c}$$

The scalar wave equation given in (III.2a) can be derived by first applying the curl operator to both sides of (III.3a). Then, the left hand side is given by the well know identity

$$\boldsymbol{\nabla} \times \boldsymbol{\nabla} \times \mathbf{E} = \boldsymbol{\nabla}(\boldsymbol{\nabla} \cdot \mathbf{E}) - \boldsymbol{\nabla}^2 \mathbf{E}.$$

The first term of this equation can be eliminated because of III.3c. Then, after applying (III.3b) in order to determine the right hand side, the following version of the scalar wave equation is derived

$$\left(\boldsymbol{\nabla}^2 - \mu_0 \epsilon_0 \partial_t^2 \right) \mathbf{E}(t, \mathbf{x}) + \mu_0 \partial_t \mathbf{J}(t, \mathbf{x}) = 0. \tag{III.4}$$

Here, applying the identity $\mu_o \epsilon_0 = c_0^{-2}$ shows that equation (III.4) is equivalent to the scalar wave equation given in (III.2a). In a similar fashion, the scalar wave equation for the magnetic field can be found using (III.1a), (III.1b), and (III.1d).

III.2 Scalar Wave Propagation Model

In the previous section, it was determined that the radar waves can be modeled by the nonhomogeneous scalar wave equation (III.4). Also, the electromagnetic field that makes up the radar wave is due to an electrical current $\mathbf{J}$ on the transmitting antenna. The vector form of the electric field and current density function $\mathbf{E}, \mathbf{J} \in \mathbb{R}^3$ can be written in terms of its components such that $\mathbf{E} = (E_1, E_2, E_3)^T$ and $\mathbf{J} = (J_1, J_2, J_3)^T$. Thus, in general, the following wave equation can be used in the place of (III.2a).

$$\left(\nabla^2 - \frac{1}{c^2(\mathbf{x})} \partial_t^2 \right) u(t, \mathbf{x}) = -j(t, \mathbf{x}). \tag{III.5}$$

In the above equations, $u = E_i$ for $1 \leq i \leq 3$. Also, $j = \mu_0 \partial_t J_i$ will denote the modified current density function, which will have compact support on the set of points located on the antenna.

In this model, the electric field can be divided into two component fields

$$u = u^{\text{in}} + u^{\text{sc}}.$$

In the above identity, $u^{\text{in}}(t, \mathbf{x})$ is the incident field that is emitted by the antennas, and u^{sc} is the scattered field, which results from the interaction of the incident field with a target. Since the source of the incident field is a current on the antenna, u^{in} is modeled using the following non-homogeneous wave equation.

$$\left(\nabla^2 - \frac{1}{c_0^2}\partial_t^2\right) u^{\text{in}}(t, \mathbf{x}) = -j(t, \mathbf{x}), \tag{III.6}$$

A wave equation that describes the propagation of the scattered field is derived from (III.5) and (III.6). This equation is given as follows

$$\left(\nabla^2 - \frac{1}{c_0^2}\partial_t^2\right) u^{sc}(t, \mathbf{x}) = -V(\mathbf{x})\partial_t^2 u(\mathbf{x}, t). \tag{III.7}$$

In equation (III.7), $V(\mathbf{x})$ is a reflectivity function, which is given by:

$$V(\mathbf{x}) = \frac{1}{c_0^2} - \frac{1}{c^2(\mathbf{x})}.$$

When the incident field comes into contact with a target, it induces a current, which causes the target to re-emit a weaker time shifted version of the same signal. However, $V(\mathbf{x})$ does not directly measure the intensity of the reflected signal. Instead, it indicates the level perturbation that occurs in the wave speed when the incident field comes in contact with the target plane. It will be assumed that the reflectivity function has compact support on the set of points on the target plane that have been illuminated by the antenna.

The solution to equation (III.6) can be determined using the Green's Function for the wave equation, which is given as follows.

$$g(t, \mathbf{x}) = \frac{\delta(t - |\mathbf{x}|/c_0)}{4\pi|\mathbf{x}|}.$$

Then, the solution for the incident field is given by:

$$u^{\text{in}}(t, \mathbf{x}) = \int_{\mathbb{R}^3} d\mathbf{y} \int_{\mathbb{R}} d\tau \frac{\delta(t - \tau - |\mathbf{x} - \mathbf{y}|/c_0)}{4\pi|\mathbf{x} - \mathbf{y}|} j(\tau, \mathbf{y}). \tag{III.8}$$

As was already stated, the modified current density function j will only have support on the set of transmitting and receiving antennas. In the case of this model, the incident field u^{in} will be produced by a single stationary isotropic point antenna $\mathbf{x}_0 \in \mathbb{R}^3$. Given this assumption, a time varying signal given by p can be introduced. This signal will be referred to as the transmitted signal, and it will be assumed to have the form given in section II.4. However, in general for radar imaging applications, other transmitted signals may be used. In most cases, FM modulated signals of the form $p(t) = a(t)e^{i2\pi f_c t}$ are used, where, f_c is the given carrier frequency. Then, the antenna current density will be modeled such that $j(t, \mathbf{x}) = p(t)\delta(\mathbf{x} - \mathbf{x}_0)$. Subsisting this into III.8 yields the following expression

$$\begin{aligned} u^{\text{in}}(t, \mathbf{x}) &= \int_{\mathbb{R}^3} d\mathbf{y} \int_{\mathbb{R}} d\tau \frac{\delta(t - \tau - |\mathbf{x} - \mathbf{y}|/c_0)}{4\pi|\mathbf{x} - \mathbf{y}|} j(\tau, \mathbf{y}) \\ &= \frac{p(t - |\mathbf{x} - \mathbf{x_0}|/c_0)}{4\pi|\mathbf{x} - \mathbf{x_0}|}. \end{aligned} \tag{III.9}$$

Furthermore, it is common to represent the current wave model in the frequency domain. Such a representation can be found by considering the following Helmholtz wave equation

$$\left(\nabla^2 + k^2\right) u^{\text{in}}(t, \mathbf{x}) = -J(\mathbf{x}, f). \tag{III.10}$$

In the above equation, u^{in} and $J(\mathbf{x}, f)$ are the Fourier transforms of u^{in} and $j(\mathbf{x}, f)$, respectively.

This equation can be solved using the Helmholtz Green's function

$$G_f(\mathbf{x}) = \frac{e^{-ik|\mathbf{x}|}}{4\pi|\mathbf{x}|}.$$

Note, in the above equation $k = \dfrac{2\pi f}{c_0}$ denotes the wavenumber. Then, the solution for the frequency domain representation of the incident field is given in terms of the following equation

$$\begin{aligned} U^{\text{in}}(\mathbf{x}, f) &= \int_{R^3} \frac{e^{-ik|\mathbf{x}-\mathbf{y}|}}{4\pi|\mathbf{x}-\mathbf{y}|} J(\mathbf{x}, f)\, d\mathbf{y} = \\ &= P(f) \frac{e^{-ik|\mathbf{x}-\mathbf{x}_0|}}{4\pi|\mathbf{x}-\mathbf{x}_0|}, \end{aligned} \tag{III.11}$$

where $U^{\text{in}}(\mathbf{x}, f)$ is the Fourier transform of $u(t, \mathbf{x})$. The definition of the Fourier transform that is used in this case is

$$H(f) = \mathscr{F}\{h\}(f) = \int_{\mathbb{R}} h(t) e^{-i2\pi f t} dt,$$

and the inverse Fourier transform is defined by

$$h(t) = \mathscr{F}^{-1}\{H\}(t) = \int_{\mathbb{R}} H(f) e^{i2\pi f t} df.$$

Given the representations of the incident field given by (III.9) and (III.11), the next step in the formulation of a model for radar wave propagation is to consider what happens when the incident field comes in contact with a target. As was previously mentioned, when the incident field comes in contact with a portion of the ground target with nonzero reflectivity, a weaker scattered version of the same wave is re-emitted. In the next section, a model for the scattered field will be found within the context of the current wave model.

III.3 The Lippman-Schwinger Equation

Since the scattered field is created as a result of the interaction of the incident field with the target scene, it would be useful if a formulation for the scattered field could be found directly in terms of the incident field. However, in general, this is not always possible. Consider that the scattered

field can be described by the following equation

$$\left(\nabla^2 + k^2\right) U^{sc}(\mathbf{x}, f) = V(\mathbf{x}) U(\mathbf{x}, f). \tag{III.12}$$

The solution to this equation can be found, in the same way as before, in the frequency domain to be

$$U^{\text{sc}}(\mathbf{x}, f) = -(2\pi f)^2 \int_{\mathbb{R}^3} \frac{e^{-ik|\mathbf{x}-z|}}{4\pi|\mathbf{x}-\mathbf{z}|} V(\mathbf{z}) U(\mathbf{z}, f)\, d\mathbf{z}, \tag{III.13}$$

and in the time domain to be

$$u^{\text{sc}}(\mathbf{x}, f) = \int_{\mathbb{R}^3} d\mathbf{z} \int_{\mathbb{R}} d\tau \frac{\delta(t - \tau - |\mathbf{x}-\mathbf{z}|/c_0)}{4\pi|\mathbf{x}-\mathbf{z}|} V(\mathbf{x}) \partial_t^2 u(\mathbf{z}, t). \tag{III.14}$$

It is clear that in both of the above expressions that the scattered field is dependent on the total field. Since in (III.13) and (III.14) the scattered field appears on both sides of the equation, it is not possible to exactly formulate the scattered field in terms of the incident field alone. In the following two sections, a solution to this problem will be detailed.

III.4 The Neumann Series Expansion

As was noted in the previous section, the scattered field appears on both sides of equation (III.13). This complicates the mathematics associated with the scattering model, since it requires an approximate solution for the total field to be found. One approach for finding such an approximation is to consider equation (III.13) in terms of a linear operator $\mathcal{L} = \mathcal{G}\mathcal{V}$. Here, $\mathcal{V}$ denotes multiplication by the reflectivity function, and $\mathcal{G}$ denotes convolution by the Green's Function for Helmholtz's Equation. Then, in terms of the operator $\mathcal{L}$, equation (III.13) becomes $U^{\text{sc}} = \mathcal{L}U$. Since $U^{\text{sc}} = U - U^{\text{in}}$, this can be rearranged to obtain the following solution for the total field U

$$U = (\mathcal{I} - \mathcal{L})^{-1} U^{\text{in}},$$

where $\mathcal{I}$ denotes the identity operator.

In general, given a linear operator $\mathcal{M}$ on a vector space X, it is often possible to expand the

operator $(\mathcal{I}-\mathcal{M})^{-1}$ in terms of the Neumann series as follows

$$(\mathcal{I}-\mathcal{M})^{-1}=\sum_{n=0}^{\infty}\mathcal{M}^n.$$

It has been show that if the Neumann series converges in the operator norm, then the operator $\mathcal{I}-\mathcal{M}$ is invertible. In general, the Neumann series converges in norm for any $\mathcal{M}$ in a Banach space such that $\|\mathcal{M}\|<1$, where $\|\cdot\|$ is the operator norm in X [8]. This is not a necessary condition for the convergence of the Neumann series, which may converge under weaker conditions.

In radar imaging applications, the Neumann series will converge when the initial scattering event is sufficiently weak. The subsequent scattering events will then have negligible power. In radar imaging, this condition is referred to as the weak scattering condition. When, these conditions are satisfied the total field can be determined using the following series expansion in terms of the incident field.

$$\begin{aligned}U=U^{\text{in}}&+\int_{\mathbb{R}^3}G_f(\mathbf{x}-\mathbf{y})V(\mathbf{y})\omega^2U^{\text{in}}(\mathbf{y})\,d\mathbf{y}\\&+\int_{\mathbb{R}^3}G_f(\mathbf{x}-\mathbf{y})V(\mathbf{y})\omega^2U^{\text{in}}(\mathbf{y})\int_{\mathbb{R}^3}G_f(\mathbf{x}-\mathbf{z})V(\mathbf{z})\omega^2U^{\text{in}}(\mathbf{z})\,d\mathbf{y}d\mathbf{z}+\dots.\end{aligned}\tag{III.15}$$

When the subsequent scattering events after the first scattering event are negligible, the series expansion above can be truncated after the first term in the expansion such that $U\approx U^{\text{in}}$. This is referred to as the Born Approximation, which will be discussed in more detail in the next section.

III.5 The Born Approximation

As mentioned in the last section, assuming that only a single scattering event occurred, or at least that any subsequent scattering events were of negligible power, the total field can be approximated by the incident field. This approximation serves to linearize the process of finding the scattered field. Given this assumption, the equation (III.13) for the scattered field in the frequency

domain then becomes:

$$\begin{aligned} U^{\text{sc}}(\mathbf{x}, f) &= -(2\pi f)^2 \int_{\mathbb{R}^3} \frac{e^{-ik|\mathbf{x}-z|}}{4\pi|\mathbf{x}-\mathbf{z}|} V(\mathbf{z}) U^{\text{in}}(\mathbf{z}, f)\ d\mathbf{z} \\ &= -(2\pi f)^2 P(f) \int_{\mathbb{R}^3} \frac{e^{-ik|\mathbf{z}-\mathbf{x}_0|} e^{-ik|\mathbf{x}-\mathbf{z}|}}{(4\pi)^2 |\mathbf{z}-\mathbf{x}_0||\mathbf{x}-\mathbf{z}|} V(\mathbf{z})\ d\mathbf{z}. \end{aligned} \tag{III.16}$$

This can also be written in terms of the following time domain representation:

$$\begin{aligned} u^{\text{sc}}(\mathbf{x}, t) &= \int_{\mathbb{R}^3} d\mathbf{z} \int_{\mathbb{R}} d\tau \frac{\delta(t - \tau - (|\mathbf{z}-\mathbf{x}_0| + |\mathbf{x}-\mathbf{z}|)/c_0)}{(4\pi)^2 |\mathbf{z}-\mathbf{x}_0||\mathbf{x}-\mathbf{z}|} V(\mathbf{z}) \partial_t^2 u^{\text{in}}(\mathbf{z}, t) \\ &= \int_{\mathbb{R}^3} \frac{\ddot{p}_n(t - (|\mathbf{z}-\mathbf{x}_0| + |\mathbf{x}-\mathbf{z}|)/c_0)}{(4\pi)^2 |\mathbf{z}-\mathbf{x}_0||\mathbf{x}-\mathbf{z}|} V(\mathbf{z})\ d\mathbf{z}. \end{aligned} \tag{III.17}$$

With this linearized approximation for the scattered field, it is now possible to model the signal that is returned to each receiving antenna. This can be accomplished by evaluating the scattered field at the antenna position $\mathbf{x}$. In the next sections, this will be examined in greater detail.

III.6 Recieved Signal

It was previously noted that the received signal, which is given by $s(t)$, can be found by evaluating the scattered field at the antenna position $\mathbf{x}_0$. In this case, the equation for the received signal is given by:

$$S(f) = U^{\text{sc}}(\mathbf{x}_0, f) = -(2\pi f)^2 P(f) \int_{\mathbb{R}^3} \frac{e^{-i2k|\mathbf{z}-\mathbf{x}_0|}}{(4\pi)^2 (|\mathbf{z}-\mathbf{x}_0|)^2} V(\mathbf{z}) d\mathbf{z}. \tag{III.18}$$

Also, the time varying version of the scattered field is given by:

$$s(t) = \int_{\mathbb{R}^3} \frac{\ddot{p}(t - 2|\mathbf{z}-\mathbf{x}_0|/c_0)}{(4\pi)^2 |\mathbf{z}-\mathbf{x}_0|^2} V(\mathbf{z}) d\mathbf{z}. \tag{III.19}$$

The computation of the incident field can be simplified by eliminating the second derivative in equation III.19. This can be accomplished by choosing the baseband signal $a(t)$, which was discussed in section II.3, such that it is slowly varying in relation to the carrier signal. Given this assumption the second derivative of the incident field can be approximated by $\ddot{p}(t) \approx -4\pi^2 f_c^2 p(t)$. For a linear chirp signal of the form given in section II.4, it would be beneficial to find a criteria

for K and T such that this condition holds. This can be done by first writing the chirp signal in equation II.5 as $p_{\text{chirp}}(t) = e^{iq(t)}$, where $q(t) = Kt^2 + 2\pi f_c t$. Next, taking the second derivative shows that

$$\ddot{p}_{\text{chirp}}(t) = \partial_t^2 e^{iq(t)} = \left\{ i\ddot{q}(t) - (\dot{q}(t))^2 \right\} e^{iq(t)}. \tag{III.20}$$

Then, computing the bracketed terms gives:

$$i\ddot{q}(t) - (\dot{q}(t))^2 = 4\pi^2 f_c^2 \left\{ -\left(1 + \frac{Kt}{2\pi f_c}\right)^2 + \frac{iK}{4\pi^2 f_c^2} \right\}. \tag{III.21}$$

From the computation above, it can be concluded that

$$\ddot{p}_{\text{chirp}}(t) \approx -4\pi^2 f^2 p_{\text{chirp}}(t),$$

when

$$\frac{K}{4\pi^2} << f_c^2 \qquad \text{and} \qquad \frac{Kt}{2\pi} << f_c.$$

Under this condition the second derivative can be omitted from (III.19), and the factor $-(2\pi f)^2$ can be dropped in (III.18). Thus, the expressions for the scattered field is

$$S(f) = U^{\text{sc}}(\mathbf{x}_0, f) = P(f) \int_{\mathbb{R}^3} \frac{e^{-i2k|\mathbf{z}-\mathbf{x}_0|}}{(4\pi)^2 (|\mathbf{z}-\mathbf{x}_0|)^2} V(\mathbf{z}) d\mathbf{z}, \tag{III.22}$$

$$s(t) = \int_{\mathbb{R}^3} \frac{p(t - 2|\mathbf{z}-\mathbf{x}_0|/c_0)}{(4\pi)^2 |\mathbf{z}-\mathbf{x}_0|^2} V(\mathbf{z}) d\mathbf{z}. \tag{III.23}$$

This model can be applied for any monostatic radar system. A model that is more specific to SAR can be found by replacing $\mathbf{x}_0$ with a time varying function $\mathbf{\Gamma}(t)$, which represents the motion of the antenna along its flight path. The range from the antenna to the target can now be characterized in terms of the function $R(\mathbf{z}, t) = |\mathbf{z} - \mathbf{\Gamma}(t)|$. The equation for the received signal can now be written as

$$S(f) = P(f) \int_{\mathbb{R}^3} \frac{e^{-i2kR(\mathbf{z},t)}}{(4\pi)^2 R^2(\mathbf{z}, t)} V(\mathbf{z}) d\mathbf{z}. \tag{III.24}$$

CHAPTER IV

CIRCULAR SAR MODEL

IV.1 Circular SAR Geometry

In chapter II, it was mentioned that the CBP algorithm is well suited to spotlight-mode SAR image formation. However, spotlight-mode SAR was developed based on early experiments with targets on a rotating turntable [26, 38]. This is referred to as turntable-ISAR. Turntable-ISAR is mathematically equivalent to the case of an antenna moving in a circular path around a fixed target. It is this case that will be considered in this section.

For the sake of mathematical simplicity, it will be assumed that the all targets lie on a flat ground topography. Hence, all will be located within a bounded subset Ω of the x_1, x_2-plane. As pictured in Figure IV.1, the antenna will move counter-clockwise along a circular path of radius r, with its center right above the origin. This flightpath will remain parallel to the ground plane with fixed height h. It will also be assumed, that the starting point of the radar platform will be located over the x_1-axis.

In the last chapter, the range from a point $\mathbf{z} \in \Omega$ was found to be $R(\mathbf{z}, t) = |\mathbf{z} - \mathbf{\Gamma}(t)|$, where $\mathbf{\Gamma}(t)$ indicates the time dependent position along the antenna path. For the flight path described by Figure IV.1, the antenna path is defined by

$$\mathbf{\Gamma}(t) = (r\cos(\omega t), r\sin(\omega t), h)^T.$$

This definition is appropriate, since the distance $d = \sqrt{r^2 + h^2}$, from the origin to the antenna remains fixed as the antenna moves along the circular path. This implies that only the angular displacement varies with respect to time. The angular displacement of the antenna is denoted by $\phi(t) = \omega t$.

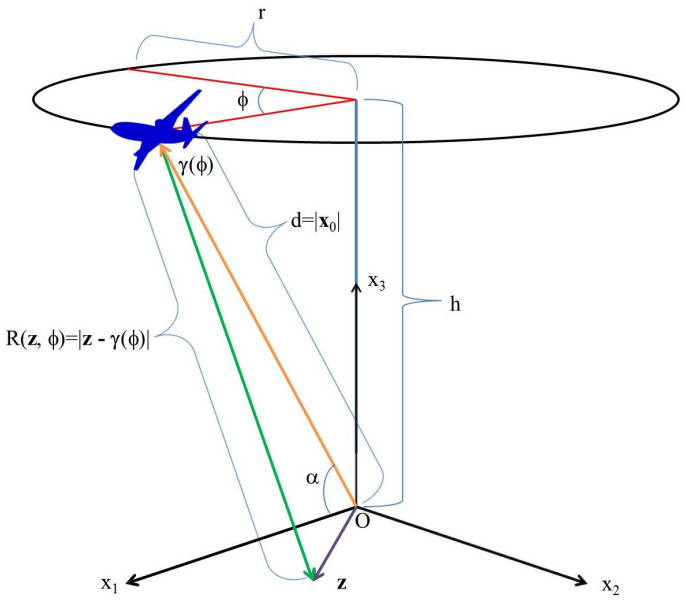

Figure IV.1: Circular SAR Geometry

In this case, the system used is a pulsed radar system. That is to say, the radar antenna will emit a series of short duration microwave pulses as it moves along its flight path. Letting t_{n_1}, t_{n_2} be the initial and final times, respectively, for the n^{th} pulse, the antenna will move from $\phi(t_{n_1})$ to $\phi(t_{n_2})$. The angular velocity ω should be small enough, in comparison to the wave speed c_0, such that the difference between $\phi(t_{n_1})$ and $\phi(t_{n_2})$ is miniscule. In this case, a single angular displacement value $\phi(t_n)$ can be used for each pulse. This is equivalent to the Start-Stop approximation that is commonly used in radar applications [7]. Then, the flight path can be represented by a function that only depends on the angle ϕ, and which is given by

$$\boldsymbol{\gamma}(\phi) = (r\widehat{\boldsymbol{\mu}}(\phi), h)^T,$$

where

$$\widehat{\boldsymbol{\mu}} \in S^1$$

. Note that S^1 is the unit sphere in $\mathbb{R}^2$ and $\widehat{\boldsymbol{\mu}}(\phi) = (\cos\phi, \sin\phi)^T$.Then, the range from the antenna

to a point $\mathbf{z} \in \Omega$ can be defined, in terms of $\boldsymbol{\gamma}(\phi)$, as

$$R(\mathbf{z}, \phi) = |\mathbf{z} - \boldsymbol{\gamma}(\phi)|.$$

IV.2 Far-Field Wave Propagation Model

Often the flight path of the radar platform is designed in such a way that the maximum target distance from the origin, which is located at the target scene center, is much smaller than the distance of the antenna from the same origin. In this case, any computation of the received signal based on equation III.24 can be simplified through the application of what is commonly referred to as the far-field approximation. This approximation can be understood by first noting that radar waves propagate as a spherical wave front. When the antenna is far from the target center, the curvature of this wavefront can be assumed to be negligible. Under this assumption, in the extreme far-field, radar wave propagation can be approximately represented by a plane wave. This assumption can be justified mathematically by applying a first order Taylor expansion to the range term $|\mathbf{z} - x_0|$

$$|\mathbf{z} - \mathbf{x}_0| = \sqrt{|\mathbf{z}|^2 + |\mathbf{x}_0|^2 - 2\mathbf{z} \cdot \mathbf{x}_0} = |\mathbf{x}_0| - \widehat{\mathbf{x}}_0 \cdot \mathbf{z} + O\left(\frac{|\mathbf{z}|^2}{|\mathbf{x}_0|}\right).$$

Then, the phase term becomes

$$e^{-ik|\mathbf{z}-\mathbf{x}_0|} = e^{-i2k|\mathbf{x}_0|} e^{i2\widehat{\mathbf{x}}_0 \cdot \mathbf{z}} \left(1 + O\left(\frac{k|\mathbf{z}|^2}{|\mathbf{x}_0|}\right)\right).$$

Similarly, the Taylor expansion can be applied to the geometric spreading factor $|\mathbf{z} - \mathbf{x}_0|^{-2}$ from the denominator of III.24 such that

$$|\mathbf{z} - \mathbf{x}_0|^{-2} = \frac{1}{|\mathbf{z}|^2 + |\mathbf{x}_0|^2 - 2\mathbf{z} \cdot \mathbf{x}_0} = \frac{1}{|\mathbf{x}_0|^2} \left(1 + O\left(\frac{|\mathbf{z}|^2}{|\mathbf{x}_0|^2}\right)\right).$$

This shows that when $|\mathbf{y}| << |\mathbf{x}_0|$ and $k|\mathbf{z}|^2 << |\mathbf{x}_0|$[1], the recieved signal can be approximately written as follows.

$$\begin{aligned} S(f,\phi) &\approx \frac{e^{-i2k|\boldsymbol{\gamma}(\phi)|}}{(4\pi)^2|\boldsymbol{\gamma}(\phi)|^2}P(f)\int_{\mathbb{R}^3} V(\mathbf{z})e^{i2k\widehat{\boldsymbol{\gamma}(\phi)}\cdot\mathbf{z}}d\mathbf{z} \\ &= \frac{e^{-i2k|\boldsymbol{\gamma}(\phi)|}}{(4\pi)^2|\boldsymbol{\gamma}(\phi)|^2}P(f)\mathscr{F}_{\mathbb{R}^3}\{V\}(-2k\widehat{\boldsymbol{\gamma}(\phi)}). \end{aligned} \tag{IV.1}$$

IV.3 Matched Filtering & Pulse Compression

The reflectivity function V could be recovered by moving all of the factors in front of the Fourier transform to the other side of equation (III.22), and then applying the inverse Fourier transform to the result

$$V(\mathbf{z}) = (4\pi)^2\mathscr{F}^{-1}_{\mathbb{R}^3}\left\{\frac{|\boldsymbol{\gamma}(\phi)|^2e^{i2k|\boldsymbol{\gamma}(\phi)|}S(f,\phi)}{P(f)}\right\}. \tag{IV.2}$$

This method of recovering the reflectivity values is commonly referred to as source deconvolution [36, 22]. In actual applications this method is impractical, since $P(f)$ is band-limited. This means that $P(f)$ is zero outside of a neighborhood with radius equal to the bandwidth. The implementation of this procedure could lead to a division by zero. However, there are several methods that are commonly used to approximate this method. For example, one common method that is often used is called deramp processing [10, 19]. This method involves multiplying the received signal by the complex quadrature form of the transmitted signal, applying a low pass filter to this product, and then taking the Fourier transform of the result. This particular method is often used to process data from Spotlight-mode SAR systems.

Deramp processing is an example of a common method, which is referred to as pulse compression[9]. The primary purpose of pulse compression is to maximize the SNR while maintaining high range resolution. Another common method of pulse compression is implemented by multiplying the received signal by the complex conjugate of the transmitted signal $\overline{P(f)}$. In order to understand why

this substitution is made, consider that, on the interval $[f_c - \frac{f_b}{2}, f_c + \frac{f_b}{2}]$,

$$\frac{1}{P(f)} = \frac{\overline{P(f)}}{|P(f)|^2}$$

Given a linear chirp signal of form in (II.5), pulse compression can be implemented by multiplying the received signal by the complex conjugate of the transmitted signal $\overline{P(f)}$. The result will then be multiplied by $(4\pi)^2|\boldsymbol{\gamma}(\phi)|$. This compensates for the power loss due to the geometric spreading that occurs as a wave moves away from its source. Also, in order to compensate for the phase offset due to the range, the pulse compressed signal should also be multiplied by the factor $e^{i2k|\boldsymbol{\gamma}(\phi)|}$. The result of these operations will be the following data function

$$\begin{aligned} D(f,\phi) &= (4\pi)^2|\boldsymbol{\gamma}(\phi)|^2 e^{i2k|\boldsymbol{\gamma}(\phi)|}\overline{P(f)S(f,\phi)} \\ &= |P(f)|^2 \int_{\mathbb{R}^3} V(\mathbf{z}) e^{i2k\widehat{\boldsymbol{\gamma}(\phi)}\cdot\mathbf{z}} d\mathbf{z} \\ &= |P(f)|^2 \mathscr{F}_{\mathbb{R}^3}\{V\}(-2k\widehat{\boldsymbol{\gamma}(\phi)}). \end{aligned} \tag{IV.3}$$

The data function is composed of a set of range profiles for every fixed value of ϕ. This will be illustrated in Chapter V.

Pulse compression is equivalent to the time domain operation known as matched filtering. A matched filter is implemented by applying the correlation of the time domain received signal with the complex conjugate of the incident wave $\overline{p(t)}$. This operation is characterized by

$$\eta_\phi(t) = \int_{\mathbb{R}} \overline{p(t')} s(\widetilde{t} - t', \phi) dt', \tag{IV.4}$$

where

$$\widetilde{t} = t - 2|\boldsymbol{\gamma}(\phi)|/c_0,$$

and

$$\eta_\phi(t) = \frac{d(t - 2|\boldsymbol{\gamma}(\phi)|/c_0, \phi)}{(4\pi)^2|\boldsymbol{\gamma}(\phi)|^2}.$$

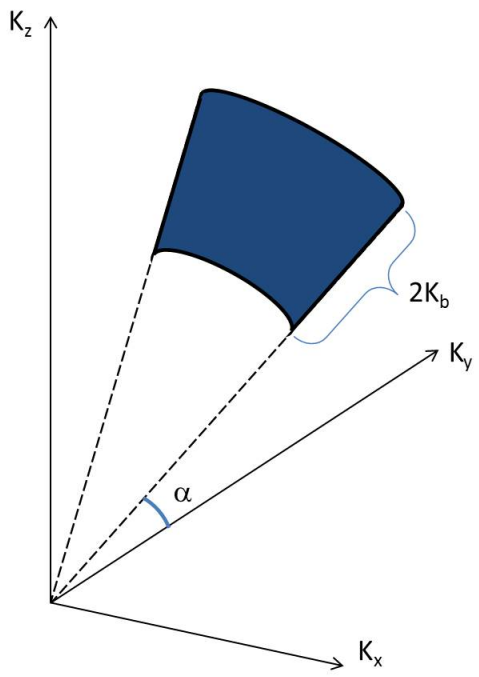

Figure IV.2: Exampe of a 3-D SAR data collection annulus on the slant plane

The main reason that the matched filter is often used in radar imaging applications is because it has been shown to optimize the SNR [7, 10].

IV.4 Data Collection

The data collection region is determined by $2k\widehat{\boldsymbol{\gamma}(\phi)}$. Hence, the shape of the data collection annulus will depend on the flight path geometry and the radar bandwith.

The function described by equation (IV.3) represents a set of radar data, which is collected in a finite region of three dimensional wavenumber domain. As is shown in Figure IV.2, the data collection region for a Circular SAR system described in Section IV.1 will be given by an annular region. This region is determined by the angular diversity of the flight path, and is located on a slant plane in the wave number space. The angle between the slant plane and the K_1, K_2-plane will be equal to the angle of inclination of the between the ground plane and the radar antenna. In addition, the length of the annular region is determined by the $K_b = \frac{2\pi f_b}{c_0}$.

In this case, the goal is to produce a two dimensional image of the target scene. For this reason, it will be necessary project the collected data onto the ground plane. This can be accomplished by

expanding (IV.3) as follows

$$\begin{aligned} D(f,\phi) &= |P(f)|^2 \int_{-\infty}^{\infty}\int_{-\infty}^{\infty}\int_{-\infty}^{\infty} V(z_1,z_2,z_3) e^{i\frac{\widetilde{k}}{d}(rz_1\cos\phi + rz_2\sin\phi + hz_3)} dz_1 dz_2 dz_3 \\ &= |P(f)|^2 \int_{-\infty}^{\infty}\int_{-\infty}^{\infty}\left[\int_{-\infty}^{\infty} V(z_1,z_2,z_3) e^{i\frac{h\widetilde{k}}{d}z_3} dz_3\right] e^{i\frac{r\widetilde{k}}{d}(z_1\cos\phi + z_2\sin\phi)} dz_1 dz_2. \end{aligned} \tag{IV.5}$$

It is now possible to define the modified reflectivity function $\widetilde{V}(\mathbf{y}) = \int_{\mathbb{R}} V(\mathbf{y}, z_3)\, e^{-i\frac{h\widetilde{k}}{d}z_3} dz_3$ where $\mathbf{y} = (z_1, z_2)^T$ and $\widetilde{k} = 2k$. Then, the expression in (IV.3) is reduced to the two-dimensional Fourier transform of the modified reflectivity function $\widetilde{V}(\mathbf{y})$

$$\begin{aligned} \widetilde{D}(f,\phi) &= |P(f)|^2 \int_{\mathbb{R}^2} \widetilde{V}(\mathbf{y}) e^{-i\widetilde{k}\widehat{\boldsymbol{\mu}}(\phi)\cdot\mathbf{y}} d\mathbf{y} \\ &= |P(f)|^2 \mathscr{F}_{\mathbb{R}^2}\{\widetilde{V}\}(\mathbf{K}). \end{aligned} \tag{IV.6}$$

Given a fixed angle ϕ, in the equation above, $\mathbf{K} = \widetilde{k}\widehat{\boldsymbol{\mu}}(\phi) = (\widetilde{k}\cos\phi, \widetilde{k}\sin\phi)^T$ corresponds to a set of lines through the origin. In the case of a single radar pulse at the angular position ϕ, the data function $\widetilde{D}(f,\phi)$ can be seen as an approximation of the Fourier transform of the reflectivity function $\widetilde{V}$ evaluated along a line corresponding to the fixed angle. The next chapter will illustrate how this idea can be used to solve the inversion problem to approximately recover the target reflectivity data in order to form a radar image. This will be accomplished through the application of the projection-slice theorem, which will be discussed in V.2

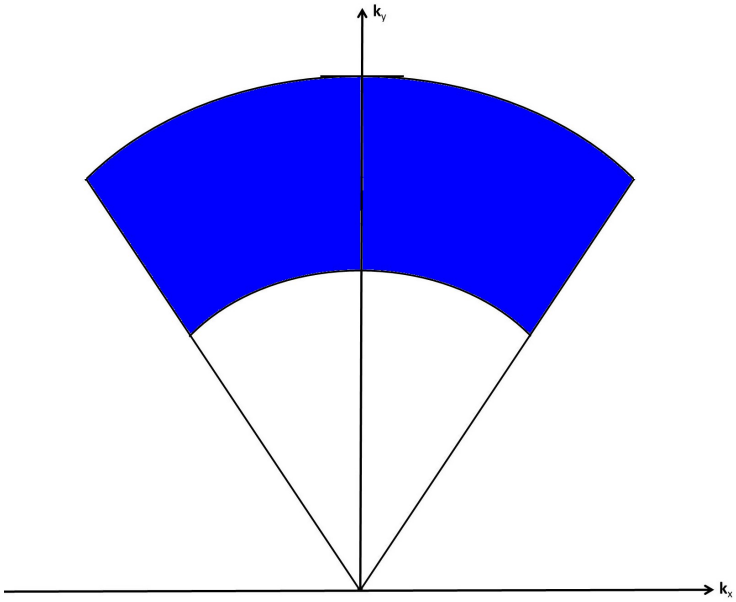

Figure IV.3: 2-D SAR data collection annulus formed by the projection of the 3-D annulus on the ground plane

In Figure IV.3, it can be seen that the data collection region corresponding to the two-dimensional imaging problem is an annular region, which is the projection of the data collection annulus in Figure IV.2 onto the ground plane in the wave number domain.

CHAPTER V

FORMULATION OF THE CBP ALGORITHM

Early imaging algorithms for spotlight-mode pulsed SAR systems used optical processing to approximately implement a two dimensional Fourier transform over a rectangular coordinate system. Recently many experts in the field have come to view radar imaging in terms of a tomographic imaging problem. As was previously mentioned, computerized tomographic imaging problems were originally studied in terms of their application to medical imaging. In the case of Computer Axial Tomography (CAT), the portion of the body that is to be imaged is illumined by a highly focused X-ray beam. This beam is passed through the patients tissue at different angular and translational orientations in order to obtain a complete image of the desired area.

The goal of any medical reconstruction algorithm is then to recover the attenuation values along each projection through the patients body. On the other hand, the goal of radar reconstruction is to accurately recover the target reflectivity function. It is not instantly apparent that the CBP algorithm is applicable to SAR. However, there is a great deal of literature, which establishes the connection between medical tomographic techniques such as the CBP algorithm and spotlight-mode SAR[12, 26]. In this chapter, the CBP algorithm is derived for the circular SAR geometry described in chapter IV.

V.1 The Radon Transform and X-Ray Transforms

In order to understand the mathematics of the CBP, it is first necessary to look at two important, but closely related, integral transforms. The first is the Radon transform, which is named after Johann Radon. The other is the X-ray transform. Both of these transforms are commonly found in inversion problems in a great variety of fields.

Conceptually, in two dimensions, the Radon transform is defined as the integral of a function f over the set of lines L in $\mathbb{R}^2$. There are a number ways in which the two dimensional Radon

transform can be defined. These definitions only differ in the way that the lines are parameterized. Initially, the Radon transform will be defined only for the set of functions $f \in \mathscr{S}(\mathbb{R}^n)$, where $\mathscr{S}(\mathbb{R}^n)$ denotes the Swartz space over $\mathbb{R}^n$. However, more generally, the Radon transform can be defined for functions in $L^2(\mathbb{R}^n)$. The Radon transform is defined in terms of integration over the set of hyperplanes in $\mathbb{R}^n$, which are given by

$$H^n_{\widehat{\boldsymbol{\mu}},s} = \{\mathbf{x} \in \mathbb{R}^n \mid \mathbf{x} \cdot \widehat{\boldsymbol{\mu}} = s\}.$$

In the above expression, $s \in \mathbb{R}$ and $\widehat{\boldsymbol{\mu}} \in S^{n-1}$, where S^{n-1} denotes the unit sphere in $\mathbb{R}^n$. In general, the output of the Radon transform of a function f on $\mathbb{R}^n$ is the function $\tilde{f}$ on the unit cylinder $C^n = \mathbb{R} \times S^{n-1}$ in $\mathbb{R}^n$. Thus, the Radon Transform can be defined as follows

$$\tilde{f}(s, \widehat{\boldsymbol{\mu}}) = \mathcal{R}\{f\} = \int_{\mathbb{R}^n} f(\mathbf{x})\delta(s - \mathbf{x} \cdot \widehat{\boldsymbol{\mu}})d\mathbf{x}. \tag{V.1}$$

In $\mathbb{R}^2$ let $\mathbf{x} = (x, y)$, and let the unit vector $\widehat{\boldsymbol{\mu}} \in S^1$ be denoted by $\widehat{\boldsymbol{\mu}}(\phi) = (\cos\phi, \sin\phi)^T$. Then for every $\mathbf{x} \in H^2_{\widehat{\boldsymbol{\mu}},\rho}$, it can be shown that there exists a constant $t \in \mathbb{R}$ such that $\mathbf{x} = s\widehat{\boldsymbol{\mu}} + t\widehat{\boldsymbol{\mu}}_\perp$, where $\widehat{\boldsymbol{\mu}}_\perp = (-\sin\phi, \cos\phi)^T$. Thus, the Radon transform is rewritten in terms of the following integral for all t.

$$\tilde{f}(s, \phi) = \int_{\mathbb{R}} f(s\cos\phi - t\sin\phi, s\sin\phi + t\cos\phi)dt. \tag{V.2}$$

The definition of the Radon transform given above clearly denotes a set of projections over lines at a various angles. At this point it is appropriate to introduce the projection function p_ϕ, which is defined below.

Definition 1. *Let f be an integrable funtion on $\mathbb{R}^2$. Then, the projection of f at a fixed angle ϕ is given by $p_\phi(s) = \tilde{f}(s, \phi)$.*

In the case of higher dimensions, the X-ray transform is used to define the projection function instead of the Radon transform. This transform is generally used in three-dimensional radar applications. The X-ray transform differs from the Radon transform in that integration is always

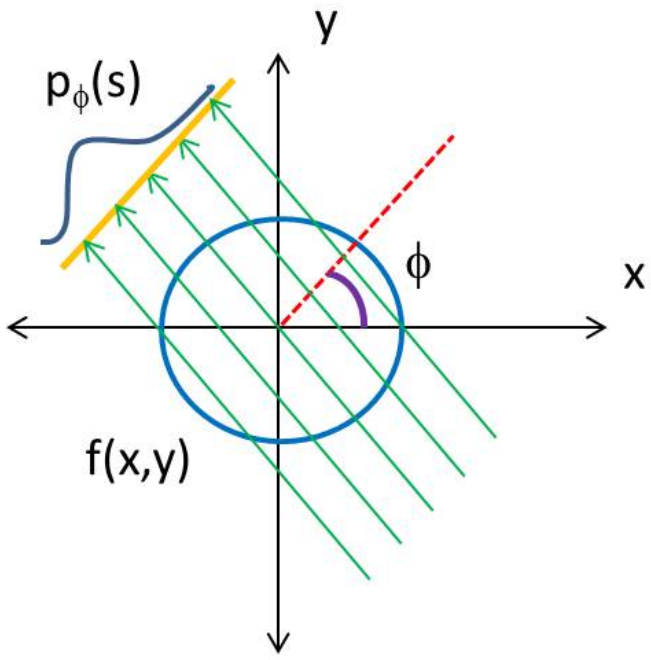

Figure V.1: Projection Function

performed over the set of lines in $\mathbb{R}^n$. However, in two dimensions there is no distinction between these two transforms. The X-ray transform is commonly used in the formulation of the three dimensional backprojection algorithms [19].

There are a number of different reconstruction methods that can be developed based on the Radon and Ray transforms. One possibility would be to reconstruct the data contained in a single projection by directly inverting the Radon or X-ray transforms, as was originally suggested by Radon himself. However, most modern backprojection algorithms are based Fourier transform inversion instead. The next section will discuss how this can be accomplished.

V.2 Projection Slice Theorem

One of the most important developments, which allowed for the creation of the CBP algorithm, is the establishment of a mathematical relationship between the Radon transform and the Fourier transform. The relationship between these two transforms is given by the Projection-Slice Theorem (PST), which was first proved in the early 1950's. This theorem can be stated is stated below[11, 28, 29].

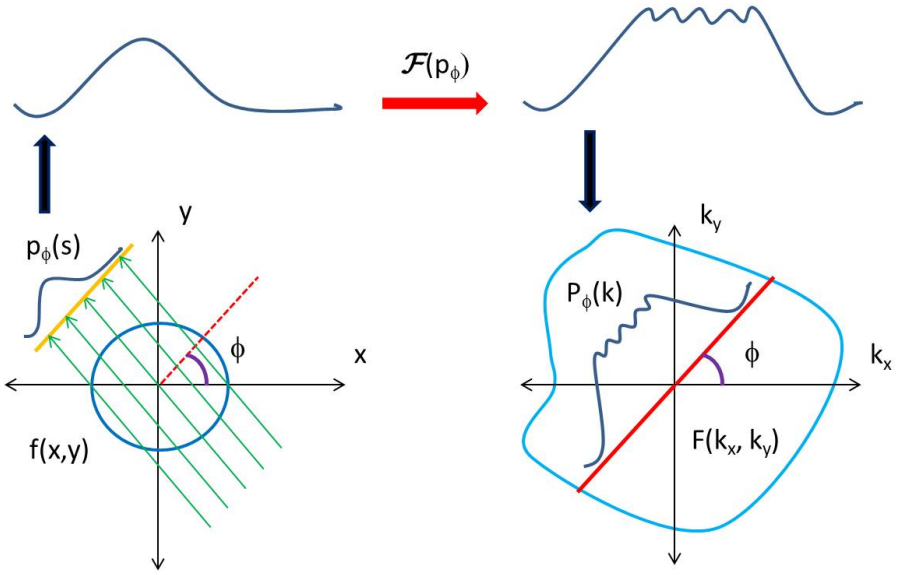

Figure V.2: The Projection Slice Theorem

Theorem 1. *Given in integrable function f on $\mathbb{R}^2$ and a fixed angle ϕ*

$$\mathscr{F}_{\mathbb{R}^2}\{f\}(s\widehat{\boldsymbol{\mu}}(\phi)) = \mathscr{F}_{\mathbb{R}}\{p_\phi\}(s).$$

Intuitively, the PST indicates that the one-dimensional Fourier transform of the projection function p_ϕ is equal to the two-dimensional Fourier transform of $f(x, y)$ along a line at angle ϕ with the K_x-axis. This relationship is can be seen in Figure V.2.

In the next section, the PST will be applied to the formulation of an inversion method for the forward model developed in Chapters III and IV. Ultimately, we will show that the radar image can be found through the inversion of Equation (IV.6).

V.3 Fourier Inversion Problem

This section will discuss how the ideas in the previous two sections are applied to formulate the CBP algorithm. In the last chapter, it was shown that when the distance from the antenna to the target scene center is much larger than the distance of each target from the same scene center, the pulse compressed version of the received signal $\tilde{D}$ is approximately equal to the Fourier transform

of the ground reflectivity function $\widetilde{V}$. Now, in order to find a reconstruction algorithm for $\tilde{V}$, let E denote Fourier transform of $\widetilde{V}$ in $\mathbb{R}^2$ such that

$$E(\mathbf{K}) = \mathscr{F}\{\tilde{V}\} = \int_{\mathbb{R}^2} \tilde{V}(\mathbf{x}) e^{-i\mathbf{K}\cdot\mathbf{x}} d\mathbf{x}. \tag{V.3}$$

The reconstructed image of the ground reflectivity function, which is denoted by I, can now be recovered by Fourier inversion of E such that $I(\mathbf{x}) = \mathscr{F}^{-1}(E)$. Next, the integral form of this expression can be written in terms of the polar coordinates $(\tilde{k}, \phi)$, where $\tilde{k} = -\dfrac{4\pi}{c_0} f$. In this case the equation for the recovered image becomes:

$$I(\mathbf{x}) = \frac{16\pi^2}{c_0^2} \int_0^{\infty} \int_0^{2\pi} E(f,\phi) e^{-i\frac{4\pi}{c_0} f(x\cos\phi + y\sin\phi)} f d\phi df. \tag{V.4}$$

In accordance with the PST, given a fixed value of ϕ, $E(f,\phi) = P_\phi(f)$, where P_ϕ represents the Fourier transform of the projections of the ground reflectivity function $\tilde{V}(\mathbf{x})$. Let $\mathbf{x} = (\rho\cos\theta, \rho\sin\theta)^T$, then the integral in equation (V.4) becomes

$$I(\rho,\phi) = \frac{4\pi}{c_0^2} \int_0^{\infty} \int_0^{2\pi} P_\phi(f) e^{-i\frac{4\pi}{c_0} f\rho\cos(\theta-\phi)} f d\phi df. \tag{V.5}$$

It is now possible to see that the name Convolution Backprojection comes from the fact that the inner integral is a circular convolution with the kernel function $L(f,\rho,\theta,\phi) = e^{-i\frac{4\pi}{c_0} f\rho\cos(\theta-\phi)}$. Generally, the CBP algorithm is not implemented in terms of equation (V.4) in its current configuration. In this case, the inner integral would be performed through a fast circular convolution algorithm. That is to say that the inner integral would be computed by

$$\text{IFFT}\left\{\text{FFT}\left\{P_\phi(f)\right\}\text{FFT}\left\{L(f,\rho,\theta,\phi)\right\}\right\}.$$

The image could then be found by summing over the set of frequent samples, along with proper polar-to-rectangular interpolation. The problem with this algorithm is that it often requires that the

kernel be sampled at a higher rate than the number of pulses. This means that an extra interpolation step must be added, which greatly reduces algorithmic efficiency. This step is referred to as the polar reformatting step, which is discussed by [3, 30, 37].

A more computationally efficient algorithm can be found by switching the order of integration in equation (V.4) so that the frequency data is processed first. In this case, the image will be given by

$$I(\rho, \phi) = \int_0^{2\pi} Q(\rho, \phi) d\phi, \tag{V.6}$$

where

$$Q(\rho, \theta, \phi) = \int_0^{\infty} P_\phi(f) e^{-i\frac{4\pi}{c_0} f\rho\cos(\theta-\phi)} f df. \tag{V.7}$$

One of the distinguishing characteristics of radar imaging is that data collected by radar systems are close approximations of the projection function in (V.7). For this reason, $P_\phi(f)$ can be replaced by the data function $\widetilde{D}(f, \phi)$, which was derived in the previous chapter. Then, $Q(\mathbf{x}, \phi)$ reads as

$$Q(\mathbf{x}, \phi) = \int_0^{\infty} \widetilde{D}(f, \phi) e^{-\frac{4\pi}{c_0} f(x_1\cos\phi + x_2\sin\phi)} f df. \tag{V.8}$$

The integral in (V.8) is generally implemented as an inverse Fourier transform over the frequency variable. Given discrete a set of radar data an IFFT is used in place of the inverse Fourier transform. The outer integral can then be implemented as a finite summation over the set angular data samples. The exact implementation of this algorithm will be discussed in detail in the next chapter.

The CBP algorithm can be used in many different SAR applications to produce high quality images as long as the antenna distance meets the criterion that is given in section IV.3. However, it does not correctly reconstruct the image in cases where the antenna is close to the target scene, which is referred to as near field imaging. This type of algorithm is important, since many experimental radar systems operate over short ranges. A near field backprojection algorithm can be found by treating III.24 as a Fourier integral operator. There are a number of sources that deal with the subject of near-field backprojection[22, 15, 31, 34].

CHAPTER VI

ALGORITHM / SIMULATION RESULTS

In the previous chapter, an inversion method, which can be used to develop a CBP algorithm, was derived. This section demonstrates how this algorithm can be implemented for a circular SAR system. Also, a series of simulations based on this algorithm will be presented.

VI.1 CBP Algorithm

The image will be recovered based on equation (V.4), which can be rewritten as

$$I(x,y) = \int_{\phi_{\text{min}}}^{\phi_{\text{max}}} Q(x,y,\phi)d\phi. \tag{VI.1}$$

In general, radar imaging systems will only record data over a small set of angular samples. This is why the integral above has been restricted to an interval between $0 \leq \phi_{\text{min}} \leq \phi \leq \phi_{\text{max}} \leq 2\pi$.

In section V.3 it was stated that the projection function can be replaced by the modified data function $\widetilde{D}(f,\phi)$. The inner integral can now be defined as follows

$$Q(x,y,\phi) = \frac{4\pi}{c^2}\int_{f_{\text{min}}}^{f_{\text{max}}} \widetilde{D}(f,\phi)e^{-i\frac{4\pi}{c_0}f(x\cos\phi+y\sin\phi)}f df. \tag{VI.2}$$

In this integral, the minimum and maximum frequencies are defined in terms of the bandwidth and the carrier frequency such that $f_{\text{min}} = f_c - \frac{f_B}{2}$ and $f_{\text{max}} = f_c + \frac{f_B}{2}$.

The actual image formation will be performed in terms of a discreet set of samples such

$$f_j = f_{\text{min}} + (j-1)\Delta f \qquad \text{for } j = 1 \ldots K,$$

and

$$\phi_m = \phi_{\text{min}} + (m-1)\Delta\phi \qquad \text{for } m = 1 \ldots N.$$

At this point, a window function is often applied to the radar data in order to suppress the effect of sidelobes on the recovered data. In this case, a Hamming window, denoted by w_N, was chosen. Then, for fixed values of j and m, the data function will be given by

$$D(f_j, \phi_m) = (4\pi)^2 d^2 \overline{P(f_j)} e^{i\frac{4\pi}{c_0} f_j d} S(f_j, \phi_m) w_H(j). \tag{VI.3}$$

In the above equation, $d = \sqrt{r^2 + h^2}$ is the distance from the antenna to the target scene center. Then, for each projection, the data can be recovered in terms of a one-dimensional IFFT.

$$Q(x, y, m) = \frac{16\pi^2}{c^2} \text{IFFT}\{f_j D(j, m)\} \Phi(x, y, m), \tag{VI.4}$$

where

$$\Phi(x, y, m) = e^{-i\frac{4\pi}{c_0} f_{\min}(x\cos\phi + y\sin\phi)}.$$

The image is recovered in terms of a summation over the set of radar pulses

$$I(x, y) = \sum_{m=1}^{N} Q(x, y, m). \tag{VI.5}$$

VI.2 CBP Algorithm Summary

The processing of a received set of radar data can be divided into two stages. First the data is pre-processed. This results in a set of data that is equivalent to $D(j, m)$. The pre-processing phase for a set of received radar data is summarized as follows:

1. Multiply by $(4\pi)^2 d^2$ to compensate for geometric spreading.
2. Multiply by $e^{i\frac{4\pi}{c_0} f_j d}$ to compensate for the range offset.
3. Apply the pulse compression factor $\overline{P(f_j)}$.
4. Apply to the window function $w_H(j)$ to each pulse to suppress sidelobes.

Given this set of pre-processed data, the CPB algorithm can be used to recover the image of the target scene. The CBP algorithm is summarized as follows:

1. Set up a 2-D imaging grid.
2. For each pulse, prepare reference table, assigning each pixel a range value.
3. Apply a 1-D IFFT to the radar data for each pulse.
4. Interpolate the resulting range profile onto the image grid.
5. Multiply by the phase correction function Φ.
6. Sum over the radar pulses to form the final image.

VI.3 CPB Simulation Results

In this section, a set of simulation results based on the CBP algorithm defined in the previous section are presented. These simulations were performed in Matlab for a target scene depicting the outline of a fighter jet sitting on a landing strip. The target scene is made up of a series of point targets located at positions $\mathbf{y}_k$ on the target plane, where $k = 1 \dots M$. Hence, the reflectivity function was implemented using the formula

$$V(\mathbf{x}) = \sum_{k=1}^{\infty} \sigma_m \delta(\mathbf{x} - \mathbf{y}_k).$$

where σ_m is the reflectivity value for each point target. Then, the received signal is implemented using the formula

$$S(j, m) = \sum_{k=1}^{\infty} \sigma_k \frac{e^{-i\frac{4\pi}{c_0} f_j R(k,m)}}{(4\pi R(k, m))^2},$$

where

$$R(k, m) = |\mathbf{y}_m - \boldsymbol{\gamma}(\phi_m)|.$$

This simulation was done with an angle inclination of $\alpha = 30^{\circ}$ with an antenna distance of 80 times the maximum target distance from the scene center. Also, the bandwidth of the transmitted signal is 400 kHz.

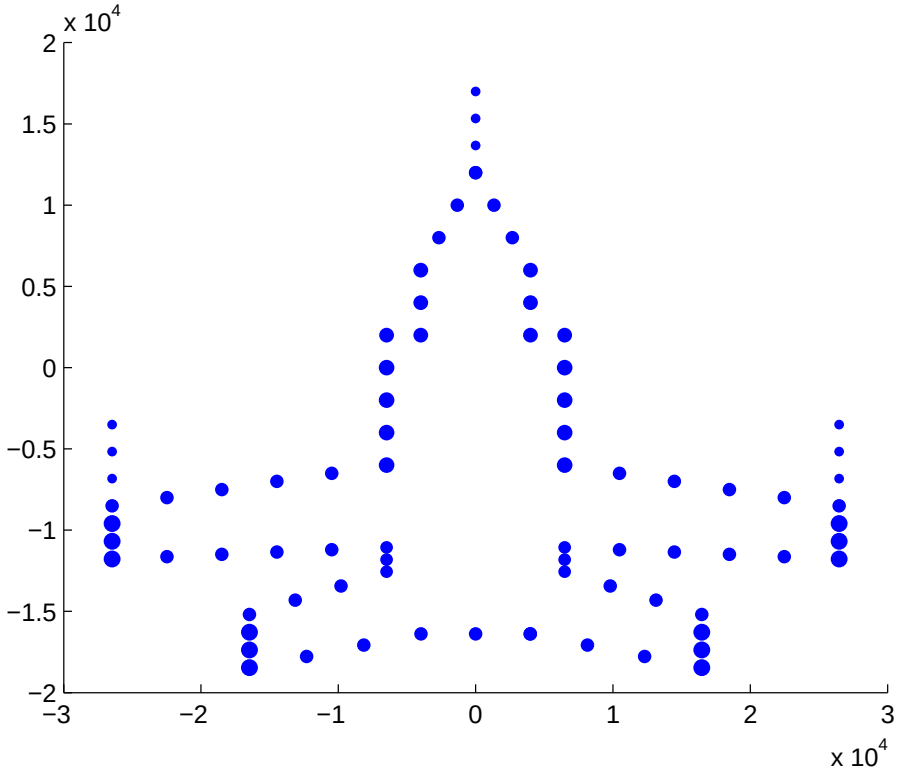

(a) Actual Target Scene

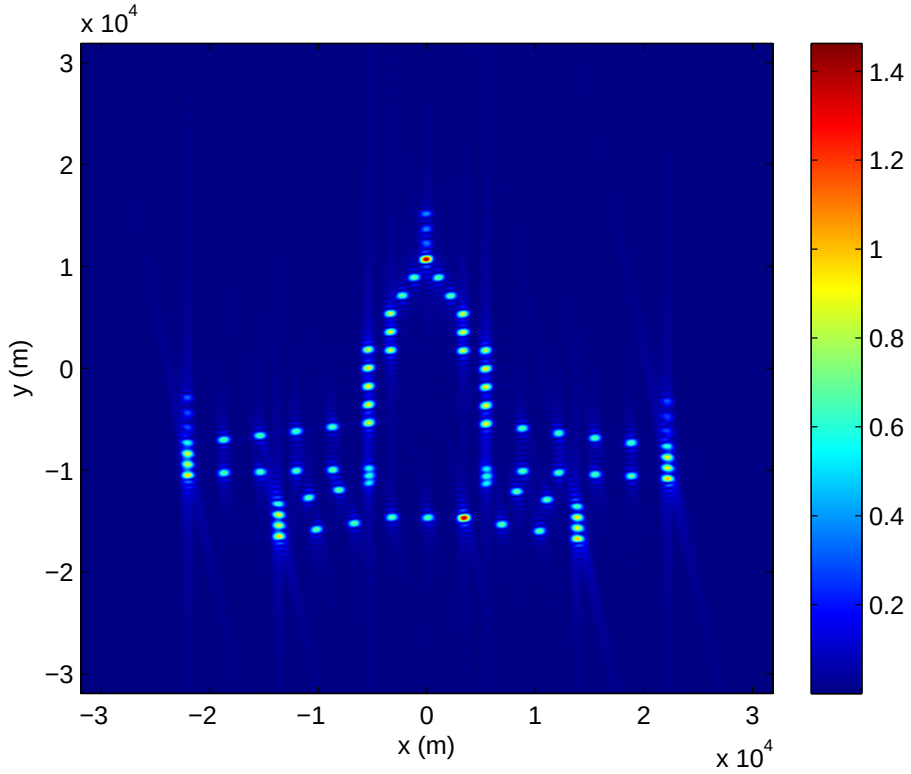

(b) CBP Image

Figure VI.1:

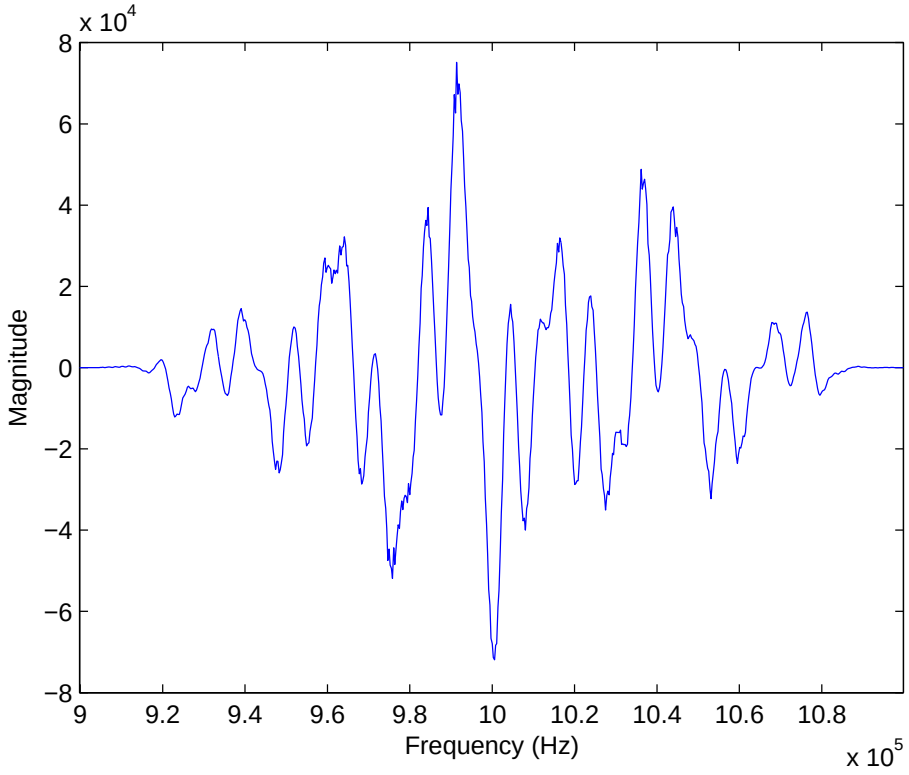

(a) Collected Data Along a Single Projection

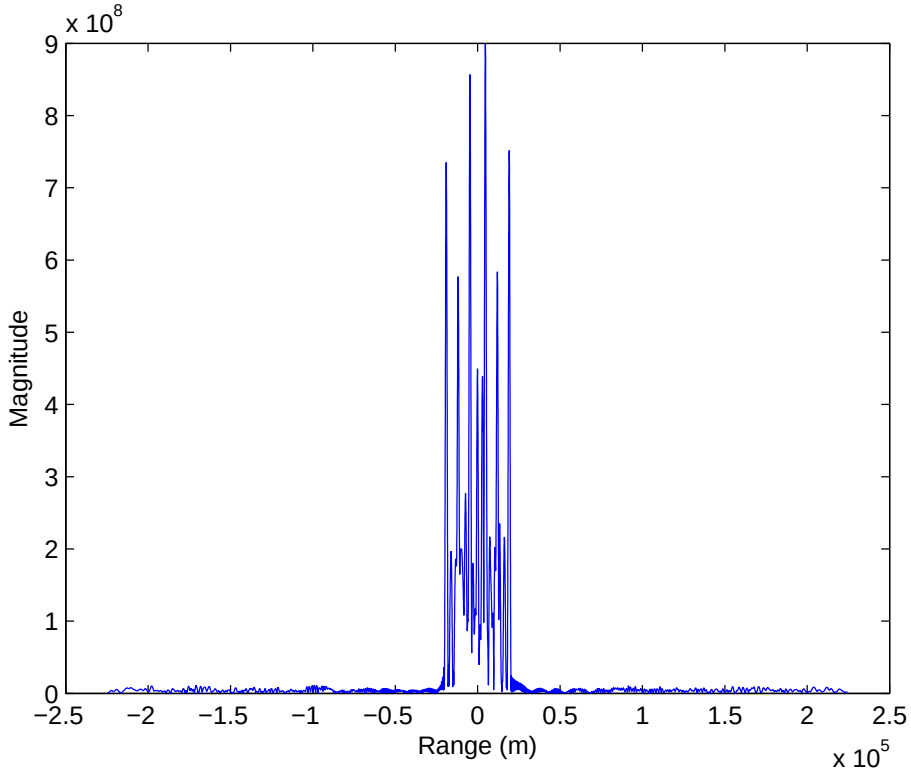

(b) Resulting Range Profile afer IFFT

Figure VI.2:

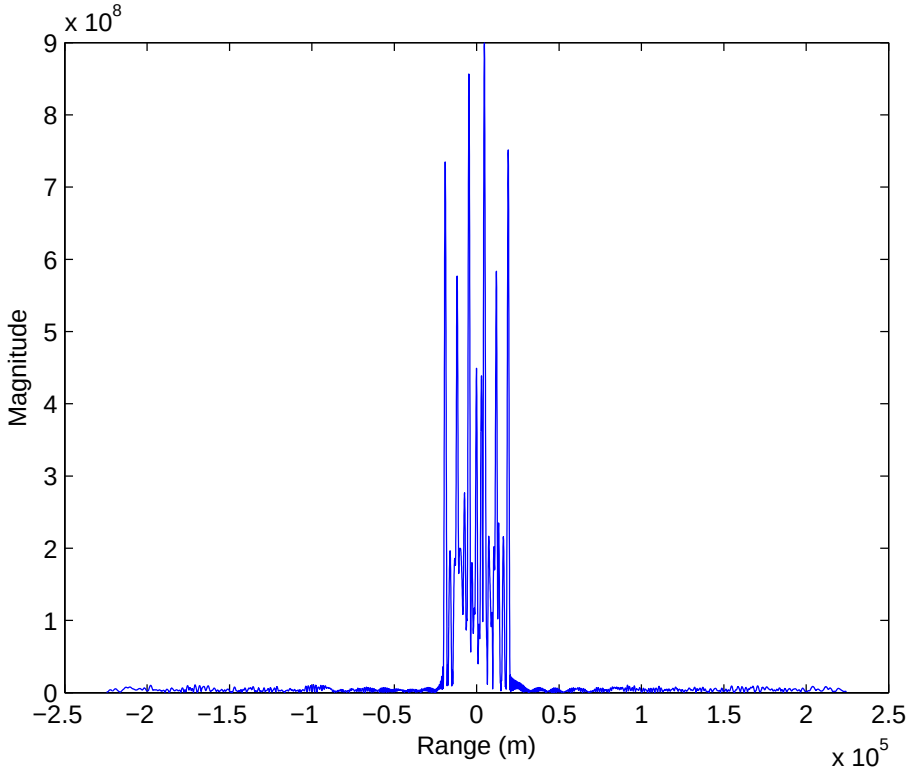

(a) Range profile prior to interpolation

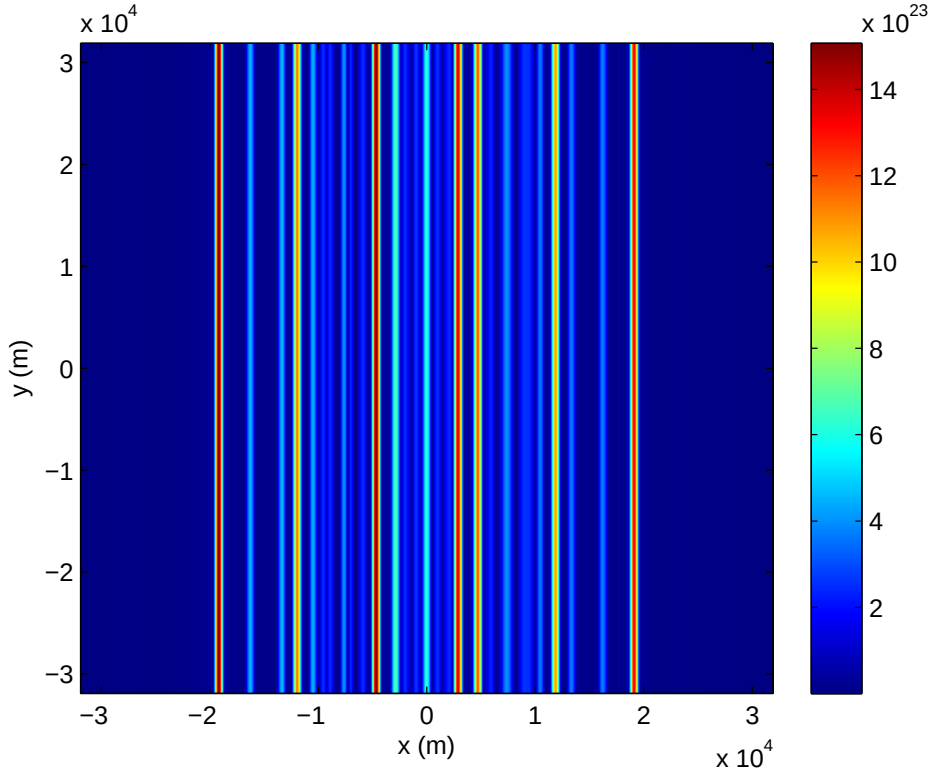

(b) Range profile interpolated to image grid

Figure VI.3:

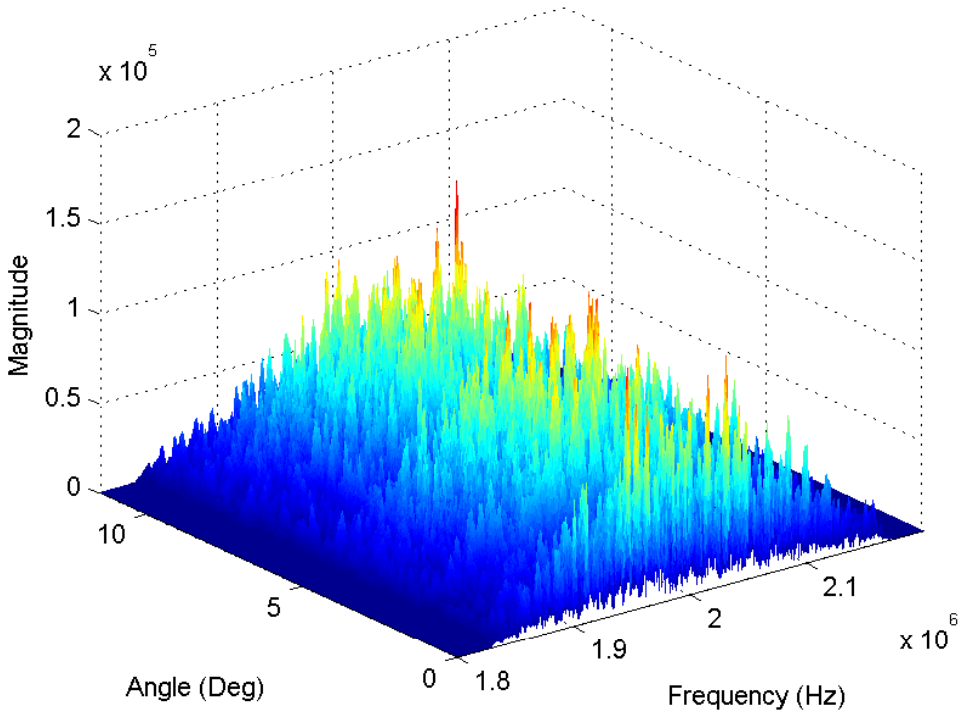

(a) Collected Data Set

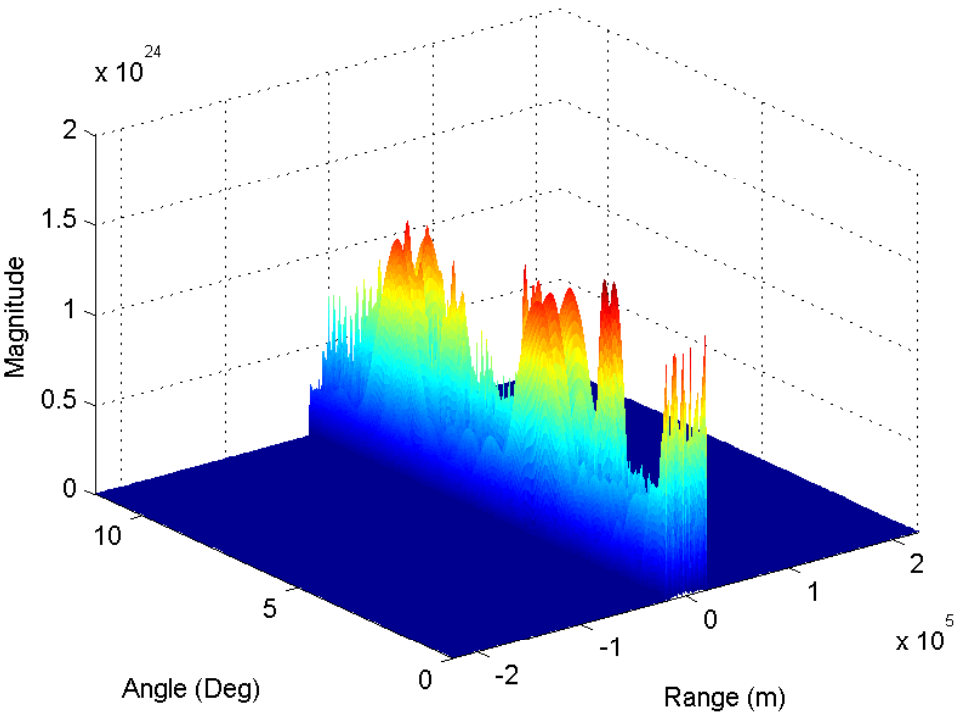

(b) Resulting Range Profile Set

Figure VI.4:

CHAPTER VII

CONCLUSION

In this thesis the convolution backprojection image formation algorithm was formulated for a circular SAR systems. In general, backprojection algorithms are used because they produce high quality images. However, this image quality comes at the expense of poor time efficiency. This method of high resolution image formation can be easily expanded to form images for spotlight-mode SAR systems. The CBP was formulated in terms of a wave model, which is based on Maxwells equations. It was shown that in the far-field the received radar data is approximately inverted using the inverse Fourier fransform. The projection-slice theorem was then used to show how the image could be accurately recovered from the set of received radar data. Finally, the ability of the CBP algorithm to produce high resolution images was demonstrated through a set of Matlab simulations.

BIBLIOGRAPHY

[1] Bauck, J. L., Jenkins, W. K., "Convolution-Backprojection Image Reconstruction for Bistatic Synthetic Aperture Radar", IEEE International Symposium on Circuits and Systems, Vol. 3, 1512 - 1515, 1989

[2] Borden, B., *Radar Imaging of Airborne Targets*. Philadelphia: Institute of Physics Publishing, 1999

[3] Broquetas, A., Palau, J., Jofre, L., Cardama, A. "Spherical Wave Near-Field Imaging and Radar Cross-Section Measurement", IEEE Transactions on Image Processing and Propgation, Vol. 46 . No. 5, 730-735 , 1998

[4] Brown, W.M., Fredricks, R.J., "Range-Doppler Imaging with Motion Through Resolution Cells", IEEE Transactions on Aerospace and Electronic Systems, Vol. 5. No. 1, 98 102, 1969

[5] Carrara, W.G., Goodman, R.S., Majeweski, R.M., *Spotlight Synthetic Aperture Radar: Signal Processing Algorithms*. Norwood, MA: Artech House, 1995

[6] Chassande-Mottin, E., Flandrin, P., "On the Stationary Phase Approximation of Chirp Spectra", Proceedings of the IEEE-SP International Symposium on Time-Frequency and Time-Scale Analysis, 117-120, 1998

[7] Cheney, M., Borden, B., *Fundamentals of RadarImaging*. Philadelphia: SIAM, 2009

[8] Cheney, W., *Analysis for Applied Mathematics*. New York: Springer-Verlag, 2001

[9] Cumming, I.G., Wong, F.H., *Digital Processing of Synthetic Aperture Radar Data*. Norwood, MA: Artech House, 2005

[10] Curlander, J.C., McDonough, R.N., *Synthetic Aperture Radar: Systems and Signal Processing*. New York: Wiley & Sons, 1991

[11] Deans, S.R., *The Radon Transform and Some of Its Applications*. New York: Dover, 1993

[12] Desai, M.D., Jenkins, K., "Convolution Backprojection Image Reconstruction for Spotlight Mode Synthetic Aperture Radar",IEEE Transactions On Image Processing, Vol. I . No. 4, 505-517, 1992

[13] Fortuny, J., Sieber, A.J., "Fast Algorithm for a Near-Field Synthetic Aperture Radar Processor", IEEE transactions on antennas and propagation, Vol. 42. No. 10, 1458-1460, 1994

[14] Franceschetti, G., Lanari, R., *Synthetic Aperture Radar Processing*. Boca Ratton, FL: CRC Press, 2000

[15] Garza, G., "Mathematics of Synthetic Aperture Radar Imaging", M.S. thesis, Dept. Math., Univ. Texas-Pan American, Edinburg, TX, 2011

[16] Garza, G., Qiao, Z., "Resolution analysis of bistatic SAR", Proceedings of SPIE Vol. 8021, 802169, 2011

[17] Gorham, L,. Moore, L., SAR image formation toolbox for MATLAB, Proceedings of SPIE, vol. 7699, 769906, 2010.

[18] Hein,A.*Processing of SAR Data Fundamentals, Signal Processing, Interferometry*. New York: Springer, 2004

[19] Jakowatz, C.,Wahl, D., Eichel, P., Ghiglia, D.,Thompson, P., *Spotlight-Mode Synthetic Aperture Radar: A Signal Processing Approach*, Norwell, MA: Kluwer Academic Publishers, 1996

[20] Kempf, T., Peichl, M., Dill, S., Suess, H., "3D Tower-Turntable ISAR Imaging", Proceedings of the 4th European Radar Confernce, 114 117, 2007

[21] Klauder, J.R., Pricel, A.C., Darlington, S., Albersheim, W.J., "The Theory and Design of Chirp Radars", The Bell System Technical Journal, Vol. 34, No. 4, 745-808, 1960

[22] Lopez, J.X., "Inverse Synthetic Aperture Radar Imaging Theory and Applications", M.S. thesis, Dept. Math., Univ. Texas-Pan American, Edinburg, TX, 2011

[23] Lopez, J.X., Qiao, Z., "Filtered back projection inversion of turntable ISAR data", Proceedings of SPIE Vol. 8051, 2011

[24] Lopez, J.X., Garza, G., Qiao, Z., "Cross-range imaging of SAR and PDE analysis", Proceedings of SPIE Vol. 7698, 76981C-1-C15, 2010

[25] Lopez, J.X., Garza, G. Qiao, Z., "Cross-Range Imaging of SAR Data", Pacific Journal of Applied Mathematics, 2(3), 65-81, 2009

[26] Munson, D.C., O'Brien, J.D., Jenkins, W.K., "A Tomogrphic Formulation of Spotlight-Mode Synthetic Aperture Radar", Procedings of the IEEE, Vol. 71, No. 8, 917-925 , 1983

[27] Munson, D.C., Sanz, J.L., Jenkins, W.K., Kakzu, G., Mather, B.C., "A Comparison of Algorithms for Polar-to-Cartesian Interpolation in Spotlight Mode SAR", IEEE International Conference on Acoustics, Speech, and Signal Processing, Vol. 10, 1364-1367, 1985

[28] Natterer, F., *The Mathematics of Computerized Tomography*. Philadelphia: SIAM, 2001

[29] Natterer, F., Wubbeling, F., *Mathematical Methods in Image Reconstruction*. Philadelphia: SIAM, 2001

[30] Nicholson, K.J., Wang, C.H., "Improved Near-Field Radar Cross-Section Measurement Technique", IEEE Antennas and Wireless Propagation Letters, Vol. 8, 1103-1106, 2009

[31] Nolan, C.J., Cheney, M., "Synthetic Aperture Inversion for Arbitrary Flight Paths and Non-Flat Topography" IEEE Transactions on Image Processing, Vol. 12, No. 9, 1035-1043, 2003

[32] Nyquist, H., "Certain Topics in Telegraph Transmission Theory", Transactions of the American Institute of Electrical Engineers, Vol. 47, No. 2, 617 - 644, 1928

[33] Prince,J.L.,"A Convolution Backprojection Formula For Three-Dimensional Vector Tomography", Proceedings of the IEEE International Conference on Image Processing, Vol. 2, 820-824, 1994

[34] Ray,T.P., Lopez, J.X., Qiao, Z., "Principles of 3D Turntable Radar Imaging", 2012 IEEE Radar Conference, 758-763, 2012

[35] Soumekh,M.*Radar Handbook*. New York: McGraw-Hill Companies, 2008

[36] Soumekh,M.*Synthetic Aperture Radar Signal Processing with MATLAB Algorithms*. New York: John Wiley & Sons, Inc., 1999

[37] Vaupel, T., Eibert, T.F., "Comparison and Application of Near-Field ISAR Imaging Techniques fiir Far-Field Radar Cross Section Determination", IEEE Transactions on Image Processing and Propogation, Vol. 54 . No. 1, 144-151, 2006

[38] Walker, J.L., "Range-Doppler Imaging of Rotating Objects", IEEE Transactions on Image Processing and Propogation, Vol. 54 . No. 1, 23 - 52, 2006

[39] Wiley, C.A., "Synthetic Aperture Radars", IEEE Transactions on Aerospace and Electronic Systems, Vol. AES-21 . No. 3, 440-443, 1985

BIOGRAPHICAL SKETCH

Timothy Paul Ray was born in Reading, PA in 1984. He attended high school at Mercer Christian Academy in Ewing, NJ. In 2010, he graduated with honors with a B.Sc. in Mathematics from the University of Texas-Pan American in 2010. Later he continued his education by earning his M.Sc. in Mathematical Sciences in 2012. From 2010-2012, he worked on the DoD Project on PDE Analysis and Radar Image Reconstruction. Timothy has a paper published in the Proceedings of the 2012 IEEE Radar Conference. He can be contacted at tpray84@gmail.com.